doi.org/10.15407/tpwj2017.05–06.12

DEVELOPMENT OF A ROBOTIC COMPLEX FOR HYBRID PLASMA-ARC WELDING OF THIN-WALLED STRUCTURES

V.N. KORZHIK[1,2], **V.N. SYDORETS**[1,2], **SHANGUO HAN**[1], **A.A. BABICH**[1,2], **A.A. GRINYUK**[2,3] and **V.Yu. KHASKIN**[1,2]

[1]Guangdong Welding Institute (China-Ukraine E.O. Paton Institute of Welding)
363 Changxing Str., Tianhe, Guangzhou 510650, China
[2]E.O. Paton Electric Welding Institute, NASU
11 Kazimir Malevich Str., 03680, Kiev, Ukraine. E-mail: office@paton.kiev.ua
[3]NTUU «Igor Sikorsky KPI»
37 Pobedi Prosp., 03056, Kiev, Ukraine

The objective of this work is development of a complex of equipment and technology of hybrid consumable electrode plasma-arc welding with coaxial wire feed for structures from steels and aluminium alloys 5–12 mm thick, using industrial robots. Mathematical modeling of processes in the arc in hybrid plasma-arc welding was the basis for selection of welding mode parameters allowing for mutual influence of the column of nonconsumable electrode constricted arc and consumable electrode arc, which enabled defining technical requirements to welding current power sources. Proceeding from mathematical and physical modeling of the process of hybrid welding, a complex of equipment and basic technologies were developed for robotic welding of thin-walled structures from steels and aluminium alloys. Developed system of complex control anabled synchronizing the functioning of two welding sources and auxiliary equipment with movements of an anthropomorphic industrial robot for realization of a stable process of hybrid consumable electrode plasma-arc welding. Application of this welding process allowed reducing electrode metal consumption by 40 %, compared to consumable electrode pulsed-arc welding at comparable speeds. Here, the level of longitudinal deflection of welded samples at hybrid process application was 3 times smaller, compared to the process of consumable electrode pulsed-arc welding. 20 Ref., 1 Table, 10 Figures.

Keywords: *robotic complex, plasma, consumable electrode arc, hybrid process, aluminium alloys, steels, welding modes, joint quality*

At present, the tendencies of welding production robotization and automation are becoming ever more urgent for large-scale production. Robot application in conveyor lines in car manufacturing can be an example of it [1]. Another important example is application of industrial robots in ship-building [2]. Here, welding robots are applied for manufacturing elements of ship hulls, deck superstructures, switching systems and diverse ship equipment [3]. The main advantage gained here is improvement of efficiency and quality of welded joints due to replacement of manual welding by automatic welding. Moreover, the requirement for highly qualified specialists–welders is reduced, and performance of high-productivity welding in difficult-of-access places becomes possible. Application of aluminium and its alloys instead of steel in ship- and car-building for manufacturing body elements allows their mass to be reduced by 50–60 %. As result, it becomes possible to increase the carrying capacity of ships and railway transport.

Well-known traditional arc processes are most often used to perform robotic welding [3]. These, primarily, are consumable (MIG/MAG) and nonconsumable (TIG) electrode welding. However, welded joints produced by these processes do not always fully meet the requirements to surface quality and level of residual deformations after welding of the produced structures. At robotization of welding processes, it is rational to apply accessible high-efficient technology, allowing minimization of the level of residual welding deformations.

One of the welding processes, which allow solving the defined task, is hybrid consumable electrode plasma-arc (Plasma-MIG) welding [4]. This process was patented for the first time in 1972 by Wilhelm Essers and other staff members of Philips Company (The Netherlands) [5]. In such a welding process, a heat source for hybrid plasma-arc welding is formed, which consists of nonconsumable electrode constricted arc, encompassing the consumable electrode arc. Additional constriction of the latter provides reduction of spatter and possibility of increasing base metal penetration depth at smaller values of electrode wire feed rate (welding current of consumable electrode

arc is smaller). Application of such a process for welded structure fabrication can provide formation of fine-grained structures of welds, as well as high quality and efficiency of welding [6].

Conventional nonconsumable pin electrode was used earlier in the designs of torches for hybrid consumable electrode plasma-arc welding. In modern designs it was replaced by hollow-annular electrode [7]. Modern modified process of hybrid plasma-arc welding has not yet become widely accepted, being, however, actively studied by researchers [8]. Technologies of welding different materials by this process are at the development stage.

The objective of this work was development of equipment and technology for hybrid consumable electrode plasma-arc welding with coaxial wire feed for robotic welding of structures from steels and aluminium alloys with 5–12 mm wall thickness.

The following tasks were solved to achieve the defined objective:

1. Modeling of the process of hybrid consumable electrode plasma-arc welding, allowing for mutual influence of nonconsumable electrode constricted arc and consumable electrode arc, which is the base for preselection of hybrid welding mode parameters.

2. Defining requirements to welding power sources.

3. Synchronizing the operation of welding sources and auxiliary equipment with anthropomorphous industrial robot.

4. Development of welding torch for hybrid plasma-arc welding, designed for continuous robotic welding.

5. Development of a robotic complex and optimization of the technology of hybrid plasma-arc welding of structures from steels and aluminium alloys with 5–12 mm wall thickness.

For preselection of parameters of the mode of hybrid consumable electrode plasma-arc welding the processes of consumable electrode heating were considered at the following assumptions (Figure 1): phases of heating of electrode extension and its melting are sufficiently well separated and interaction proceeds so that final heating conditions are initial conditions for melting; electrode extension is heated by plasma of discharge with nonconsumable electrode and welding current; molten zone length is much smaller than electrode extension length; and electrode metal transfer is of drop type. These assumptions coincide with those made in [9]. Therefore, the mathematical model was constructed similarly. The difference between MIG and Plasma-MIG welding processes consists in that electrode extension is additionally heated by plasma of discharge with nonconsumable annular electrode (anode).

Electrode wire is located inside the plasma discharge along its axis. Its temperature rises due to convection and radiation heating. Considering that plasma temperature T_p = 5500–15000 K, it is easy to show that the fraction of energy supplied to electrode wire through convection heating, is extremely small. Therefore, we did not allow for convection heating, when solving the heat problem. Radiation heating obeys Stefan-Boltzmann law, and differential equation, describing the change of temperature T in time t, has the following form:

$$\frac{dT}{dt} = \frac{2\beta\sigma_{SB}}{\gamma c r_w}\left(T_p^4 - T^4\right), \qquad (1)$$

where σ_{SB} is the Stefan–Boltzmann constant; β, γ, c, r_w are the degree of blackness, specific heat conductivity, electrode wire radius, respectively.

Solution of differential equation (1) has an implicit form:

$$t = \frac{\beta\sigma_{SB}T_p^3}{\gamma c r_w}\left[\operatorname{atanh}\left(\frac{T}{T_p}\right) - \operatorname{atanh}\left(\frac{T_0}{T_p}\right) + \operatorname{atan}\left(\frac{T}{T_p}\right) - \operatorname{atan}\left(\frac{T_0}{T_p}\right)\right], \qquad (2)$$

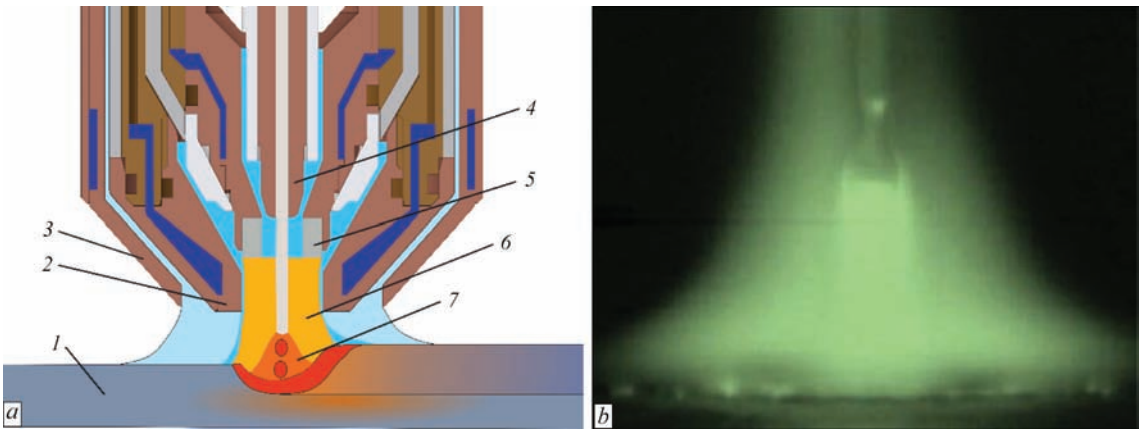

Figure 1. Technological schematic of the process (*a*) and photo of simultaneous action of constricted arc and consumable electrode arc (*b*) in hybrid plasma-arc welding: *1* — sample being welded; *2* — plasmaforming nozzle; *3* — shielding nozzle; *4* — consumable electrode nozzle; *5* — plasmatron annular electrode (anode); *6* — constricted direct arc; *7* — consumable electrode arc

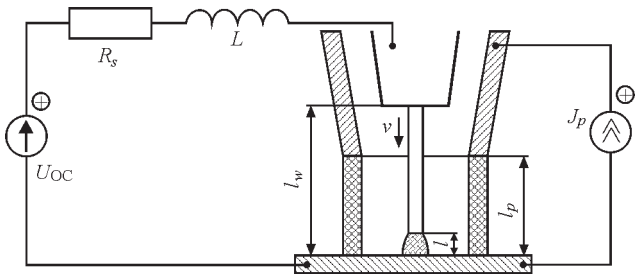

Figure 2. Schematic of connection of power sources in hybrid plasma-arc welding process

where T_0 is the initial temperature of electrode wire.

It is difficult to use solution (2) for further studies. It is simplified, considering that electrode wire melting temperature T_m is much smaller than plasma temperature T_p. In this case we obtain a simple solution

$$T = T_0 + \frac{2\beta\sigma_{SB}T_p^4}{\gamma c r_w}t. \qquad (3)$$

Difference between the solutions at melting temperature T_m is equal to 0.2 for steel and 0.02 % for aluminium (1.2 mm electrode wire diameter). This provided a base for us for further application of formula (3).

Energy accumulated in the metal of electrode extension due to welding current passage, and plasma radiation, summing up with energy evolving in near-electrode (near-cathode) region, is consumed for metal heating and melting. Electrode melting rate can be derived from this condition:

$$v_m = \frac{\pi r_w^2 U_c i + \rho i^2 (l_w - l) + 2\pi^2\beta\sigma_{SB}T_p^4 r_w^3 (l_p - l)}{\pi^2\gamma r_w^4 \left[c(T_m - T_0) + \lambda \right]},$$

where i is the welding current (MIG process current); l is the arc length; U_c is the cathode voltage drop; l_w, l_p are the distance from the tip to the item and from plasmatron nozzle to the item (Figure 2); ρ, λ are the specific resistance and latent heat of electrode metal melting.

It is obvious that electrode melting dynamics is described by differential equation, the essence of which consists in that the change of arc length is equal to the difference of electrode melting rate and electrode feed rate v

$$\frac{dl}{dt} = \frac{\pi r_w^2 U_c i + \rho i^2 (l_w - l) + 2\pi^2\beta\sigma_{SB}T_p^4 r_w^3 (l_p - l)}{\pi^2\gamma r_w^4 q} - v, \qquad (4)$$

where $q = c(T_m - T_0) + \lambda$.

In keeping with Kirchhoff's law, open-circuit voltage U_{OC} of the power source is equal to the sum of voltage drops across the circuit elements (see Figure 2) — ohmic resistance R_S and inductance L of the power source and connecting cables, ohmic resistance of electrode extension and arc voltage drop El (E is the electric field resistance in the arc)

$$U_{OC} = R_S i + L\frac{di}{dt} + \rho\frac{l_w - l}{\pi r_w^2} i + El + U_{an} + U_c, \qquad (5)$$

where U_{an} is the anode voltage drop.

Equations (4) and (5) make up a system of nonlinear differential equations, which describe the dynamics of «power source–consumable electrode arc» system during the process

$$\begin{cases} \dfrac{dl}{dt} = \dfrac{\pi r_w^2 U_c i + \rho i^2 (l_w - l) + 2\pi^2\beta\sigma_{SB}T_p^4 r_w^3 (l_p - l)}{\pi^2\gamma r_w^4 q} - v \\ \dfrac{di}{dt} = \dfrac{1}{L}\left(U_{OC} - R_S i - \rho\dfrac{l_w - l}{\pi r_w^2} i - El - U_{an} - U_c \right) \end{cases}. \qquad (6)$$

In order to find special points, which determine the static state, it is necessary to equate the right-hand parts of system (6) to zero. Equations for determination of static values of arc length l_0 and welding current i_0, have the following form:

$$\rho\left(r_w E^2 + 2\rho\beta\sigma_{SB}T_p^4\right) l_0^3 - \rho\Big[r_w E\left(2\bar{U}_{OC} + U_c + El_w\right) + 4\beta\sigma_{SB}T_p^4\left(\pi r_w^2 R_S + \rho l_w\right) + \rho\left(2\beta\sigma_{SB}T_p^4 l_p - \gamma q v r_w\right)\Big] \times$$
$$\times l_0^2 + \Big[\Big[r_w U_c E + 2\rho\left(2\beta\sigma_{SB}T_p^4 l_p - \gamma q v r_w\right)\Big] \times$$
$$\times\left(\pi r_w^2 R_S + \rho l_w\right) + \rho r_w \bar{U}_{OC}\left(\bar{U}_{OC} + U_c + 2El_w\right) + 2\beta\sigma_{SB}T_p^4\left(\pi r_w^2 R_S + \rho l_w\right)^2\Big] l_0 -$$
$$-\Big[r_w U_c \bar{U}_{OC}\left(\pi r_w^2 R_S + \rho l_w\right) + \rho r_w \bar{U}_{OC}^2 l_w + \left(2\beta\sigma_{SB}T_p^4 l_p - \gamma q v r_w\right)\left(\pi r_w^2 R_S + \rho l_w\right)^2\Big] = 0;$$
$$\rho R_S i_0^3 - \rho\left(\bar{U}_{OC} + U_c - El_w\right) i_0^2 + \pi r_w\Big[2\beta\sigma_{SB}T_p^4\Big[\pi r_w^2 R_S + \rho\left(l_w - l\right)\Big] + r_w\left(U_c E + \gamma\rho q v\right)\Big] i_0 - -\pi^2 r_w^3 \times$$
$$\times\Big[2\beta\sigma_{SB}T_p^4\left(\bar{U}_{OC} - El_p\right) + \gamma q v E r_w \Big] = 0,$$

where

$$\bar{U}_{OC} = U_{OC} - U_{an} - U_c.$$

To study the properties of these solutions let us use conditions of existence, the essence of which is as follows: Plasma-MIG process can be physically realized, when static welding current is greater than zero

$$i_0 > 0, \qquad (7)$$

and static value of arc length is in the range from zero (electrode contact with the item) up to the distance from the nozzle to the item (electrode burning-off)

$$0 < l_0 < l_w. \qquad (8)$$

Application of these conditions allows determination of maximum plasma temperature at which Plasma-MIG process proceeds

$$T_{p\max} = \left(\frac{\gamma q v E r_w}{2\beta\sigma_{SB}\left(El_p - U_{OC} + U_{an} + U\right)} \right)^{1/4}.$$

Our assessments showed that maximum temperature for steel is T_{max} = 7960 K; for aluminium

it is $T_{p\,max}$ = 7340 K (process parameters, for which calculations were performed, are given in [10]). This result is in good agreement with experimental results of temperature measurement [11].

In hybrid Plasma-MIG process mutual effect of gas discharges on each other is in place. Impact of plasma discharge on electrode wire melting was considered above. Electrode wire melting, in its turn, influences the electric parameters of plasma discharge [12, 13], in particular, its volt-ampere characteristic (VAC). These features were taken into account at selection of power sources and development of equipment for Plasma-MIG process [14]. However, dependence of electrical characteristics on technological parameters of Plasma-MIG process cannot be derived at application of currently available resistive models [15].

Arc model developed at PWI was improved to describe plasma discharge of hybrid Plasma-MIG process [16, 17].

Plasma arc is considered phenomenologically as heat macroobject, which is the element of electric circuit with static VAC $U_p(i)$. The law of energy conservation for such a heat macroobject has the following form

$$\frac{dQ}{dt} = P - P_\theta.$$

This law connects three energy parameters of plasma arc column: internal energy Q, applied P and removed P_θ power. Internal energy of arc column Q is the sum of all the plasma energies: energy of thermal motion, ionization energy, vibrational and rotational energy of molecules, etc., and it depends on arc radius and length, i.e. on its volume. By the term applied power P we mean power consumed from the power source, and by the term removed power P_θ we mean the power, which the arc column releases into the environment through heat conductivity and radiation.

Application of the term of state current [16] and introduction of variable i_θ enables expressing arc energy parameters through electric parameters

$$P = \frac{U_p\left(i_\theta\right)}{i_\theta} i_p^2, \quad P_\theta = U_p\left(i_\theta\right) i_\theta,$$

$$Q = 2\theta \int_0^{i_\theta} U_p\left(i_\theta^*\right) di_\theta^*,$$

where i_p is the plasma arc current; θ is the plasma arc time constant) and deriving the differential expression of the model

$$\theta \frac{di_\theta^2}{dt} + i_\theta^2 = i_p^2. \qquad (9)$$

Equation (9) is complemented by a formula of relation between plasma arc current and its voltage

$$u = \frac{U_p\left(i_\theta\right)}{i_\theta} i_p,$$

which is part of equation corresponding to Kirchhoff laws.

In the case of plasma arc with gas blowing, an additional mechanism of energy scattering is in place, alongside natural convection. This mechanism is based on forced convection, the power of which P_v can be allowed for directly

$$P_v = \frac{W_A}{V_A} Q = \frac{v_{ShG}}{l_p} Q,$$

where V_A is the volume taken up by plasma arc column; W_A is the volume of plasma consumed per a unit of time for longitudinal blowing $W_A = \pi(r_{Aout}^2 - r_{Ain}^2)v_{ShG}$, v_{ShG} is the speed of blowing with shielding gas; r_{Ain} and r_{Aout} are the inner and outer radii of plasma discharge column.

Power balance equation in this case becomes

$$\frac{dQ}{dt} = P - P_\theta - P_v.$$

Equation of the model of an arc with longitudinal blowing is as follows

$$\theta \frac{di_\theta^2}{dt} = i_p^2 - i_\theta^2 \left[1 + \frac{v_{ShG}}{l_{pl}} \frac{Q}{P_\theta}\right] \qquad (10)$$

It is promising to use equation (10) to describe the dynamics of plasma arc, where longitudinal blowing with shielding gas is an essential part of the process.

When electrode wire moves inside the cylindrical plasma discharge, there appears one more mechanism of energy removal, associated with its heating. It should be taken into account in the law of energy conservation.

$$\frac{dQ}{dt} = P - P_\theta - P_v - P_w.$$

Electrode wire heating due to plasma discharge radiation was considered above. Using these results, we obtain the following formula for power

$$P_w = 2\pi r_w \beta \sigma_{SB} T_p^4 \left(l_p - l_0\right).$$

Equation of generalized dynamic model of plasma arc for Plasma-MIG process has the following form

$$\theta \frac{di_\theta^2}{dt} = i_p^2 - i_\theta^2 \left(1 + \frac{P_v + P_w}{P_\theta}\right).$$

To obtain plasma discharge VAC in Plasma-MIG process we will use the procedure described in paper [18]. As a result, a parametric dependence of plasma discharge voltage on its current was derived (Figure 3)

$$U_{\text{Plasma-MIG}}\left(i_\theta\right) = U\left(i_\theta\right)\left(1 + \frac{P_v + P_w}{P_\theta}\right)^{1/2};$$

$$I_{\text{Plasma-MIG}}\left(i_\theta\right) = i_\theta\left(1 + \frac{P_v + P_w}{P_\theta}\right)^{1/2}.$$

In these formulas i_θ variable has the role of a parameter.

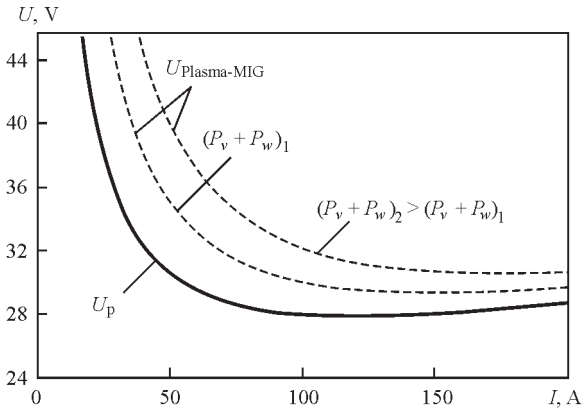

Figure 3. VAC of plasma discharge in Plasma-MIG process (*dashed lines*) compared to VAC of plasma discharge without MIG process (*solid line*)

The graph presented in Figure 3, demonstrates the tendency to voltage rise in plasma discharge in Plasma-MIG process. This is in good agreement with the phenomena, which were observed during technological experiments at comparison of Plasma and Plasma-MIG processes [10, 19, 20].

Proceeding from the conducted calculations, specification for design or selection of welding power sources has been developed. So, it is determined that power source of plasma component should provide the possibility of running of nonconsumable electrode constricted arc at reverse polarity direct current with current load from 50 up to 250 A and up to 45 V arc voltage. Power source of consumable electrode arc should provide welding current from 10 up to 350 A at 100 % duty cycle. Here, the power sources should have the capability of communication with the control system via bus interface, using the most common communication protocols. Technical requirements were the basis to select welding inverter sources, the most suitable to the developed specification. These sources are fitted with bus interface for exchange of control and feedback signals with the overall control system of the complex. For reliable operation of plasma module in RPDC welding mode, reconnection of pilot arc connectors was performed to ensure its excitation at reverse polarity. Control system of welding power sources and plasma module is based on programmable PLC controller, it provides an algorithm of sequential switching on and off of electric components of the complex of equipment for hybrid consumable electrode plasma-arc welding, acquisition of data on the welding mode, monitoring of parameters of the complex component operation for possible emergencies (Figure 4). Communication between the power sources proceeds via buses by CAN bus protocol. Algorithm of the sequence of switching-on the components of equipment complex uses current and voltage feedback signals, generated by power sources.

A typical algorithm for the process of hybrid consumable electrode plasma-arc welding is as follows: when power is applied to welding current sources, «Ready for work» signals are generated, and they come to control system controller. In the absence of the signal, further process of switching-on is blocked. When «Welding start» command is issued, the signal passes via the bus to power source of consumable electrode arc, which is followed by arc excitation. When consumable electrode arc is running, «Main current» signal from consumable electrode power source to control system controller is formed. When this signal is received, a command is generated for plasma module for arc excitation. After pilot arc excitation, a signal is generated with a time delay for excitation of the arc by plasma component power source. At excitation of nonconsumable electrode constricted arc by plasma component power source, «Main current» signal is generated, which is sent to control system controller. After passing of «Main current» signal from plasma component power source, starting of the system of displacement of the torch or the part proceeds with the selected time delay. Absence or removal of each of «Main current» signals during the process is a signal for interruption of the algorithm of switching-on the power sources, and the hybrid consumable electrode plasma-arc welding process proper.

The system performs control of external displacement devices (welding column, welding rotator, or other device), or provides interaction of the complex of welding power sources with welding robot controller and synchronizing of welding cycle stages with its actions. The main technical characteristics of robotic complex of hybrid plasma-arc welding equipment (Figure 5) are given below.

Main technical characteristics of equipment complex for hybrid plasma-arc welding

Voltage of three-phase AC mains with 50 Hz frequency, V	400 (±15 %)
Working voltage of consumable electrode arc, V	0–50
Working current of consumable electrode arc in hybrid plasma-arc welding, A	50–250
Working voltage of plasma welding source, V	15–34
Limits of regulation of different-polarity asymmetrical current, A	10–350
Limits of regulation of straight and reverse polarity direct current, A	10–350
Limits of regulation of the duration of current flowing at straight polarity, %	15–85
Shielding gas	Ar, Ar + He
Plasma gas in hybrid welding torch	Ar
Working gas pressure at power source input, MPa	0.2–0.4
Gas flow rate, l/min:	
shielding	10–40
central	1–10
plasma	0.1–10.0
Filler and electrode wire diameters, mm	1.2; 1.6

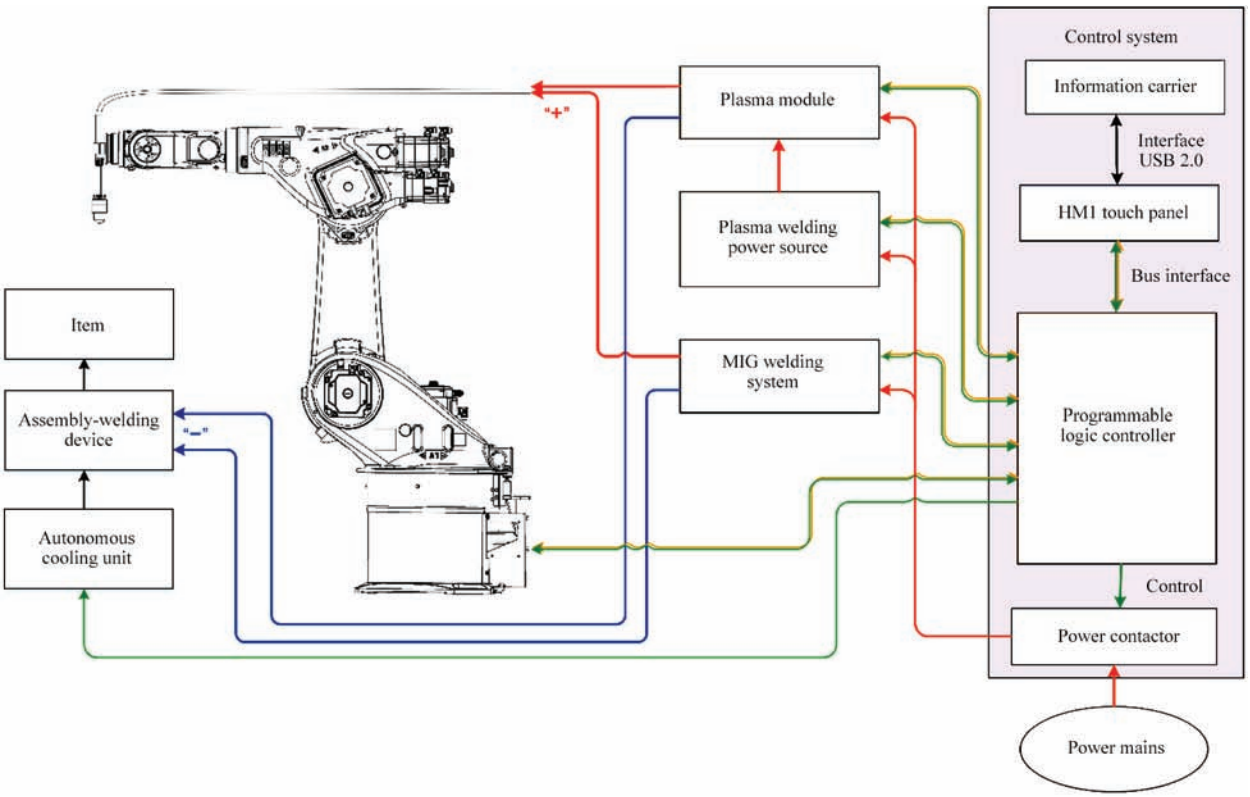

Figure 4. Block-diagram of robotic complex of hybrid plasma-arc welding

Application of bus interface, operating by CAN bus protocol, is envisaged for communication with robot controller. The problem of interaction of control system of the complex of hybrid consumable electrode plasma-arc welding equipment and robot controller is based on «Master–Slave» principle. Robot controller acts as «Master». After switching on the control system of welding equipment complex, a survey of readiness for work and serviceability of power sources is performed. In the absence of malfunction signals, «Ready» signal is formed and sent to robot controller. The robot controller at «Welding start» command moves the welding torch to the point of welding start, and transfers the command to the controller of control system of welding equipment complex to start the algorithm of arc excitation at hybrid plasma-arc welding. Control system starts the algorithm of hybrid arc excitation, and after passage of «Main current» signals, issued by power sources at arc excitation, it generates a signal for robot controller to start welding head movement by a program, installed on robot controller. After the torch has reached the welding

Figure 5. Equipment of the complex for robotic hybrid Plasma-MIG welding: *a* — control panel of the complex for hybrid Plasma-MIG welding; *b* — power sources for plasma and arc components with wire feed mechanisms; *c* — welding torch in the arm of KR 60 HA robot of KUKA Company (Germany)

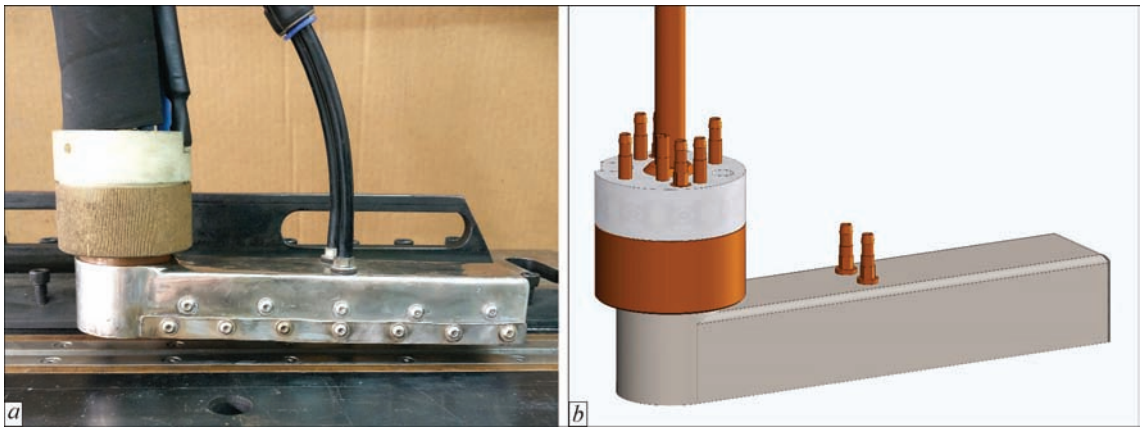

Figure 6. Appearance (*a*), and schematic (*b*) of the torch for robotic hybrid plasma-arc welding with additional shielding nozzle

end point, the controller stops movement, and issues a command to the controller of welding equipment complex control system for extinguishing the hybrid arc. Control system controller performs disconnection of power sources and plasma module by an algorithm installed in it. After removal of «Main current» signal from consumable electrode power source and completion of welding cycle, a signal is transferred to robot controller to bring the welding torch back to the initial point.

This algorithm of interaction of the system of control of the complex of welding equipment for hybrid consumable electrode plasma-arc welding and welding robot controller enables simplifying the process of welding equipment integration with robots of different manufacturers. Here, the robot controller takes over the functions of monitoring the welding tool movement; it also issues commands to control system of welding equipment complex for welding arc excitation and extinction in hybrid plasma-arc welding.

A welding torch with an assembly of additional gas shielding was developed to produce sound welds (Figure 6). Diameters of replaceable plasmaforming nozzles were selected in the range of 6–10 mm. Anode design was composite, consisting of a copper body with refractory (tungsten) insert. A hole is made in the tungsten for electrode wire feed. Working distance between plasmaforming nozzle and sample being welded should be equal to 6.0 mm. This distance was selected from the conditions of existence (7) and (8) that ensured variation of the length of electrode extension (distance from current-conducting tip for electrode wire to the item) in the range of 16–18 mm. Here, minimum spatter deposition on plasmaforming and shielding nozzles of plasmatrons in hybrid plasma-arc welding is achieved.

To optimize the technology of robotic hybrid plasma-arc welding of structures from steels and aluminium alloys 5–12 mm thick, samples of butt joints of 400×200×δ mm size from SUS304 steel (δ = 12 mm), Steel 20 (δ = 10 mm) and aluminium alloys 5083 (δ = 8.0 mm) and 1561 (δ = 8.0 mm) were prepared. Welding was performed without edge preparation. Removable backing was used to form the root part of the weld: for steels — copper, water-cooled, with 4×1.5 mm groove size; for aluminium alloys — from non-magnetic austenitic steel with groove dimensions of 8×3.0 and 6×2.0 mm. Sound weld formation was the criterion for final selection of the welding mode (Figures 7–10). To determine presence or absence of internal pores, produced samples were subjected to X-ray inspection. This resulted in determination of the modes of robotic hybrid consumable electrode

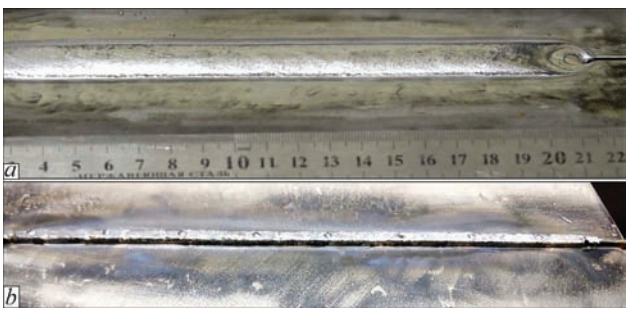

Figure 7. Butt joint of SUS304 steel (δ = 12 mm), produced by hybrid Plasma-MIG welding in the developed robotic complex: *a* — upper bead; *b* — lower bead

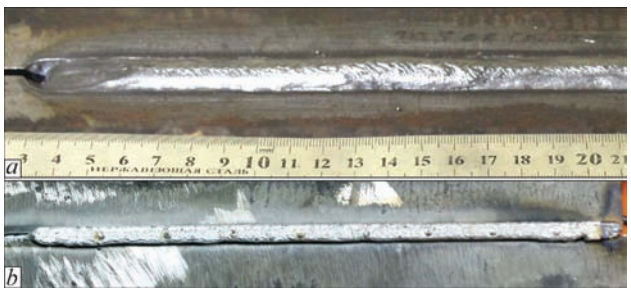

Figure 8. Butt joint of steel 20 (δ = 20 mm), produced by hybrid Plasma-MIG welding in robotic complex; *a* — upper bead; *b* — lower bead

Parameters of the modes of hybrid plasma-arc welding (Plasma-MIG) of steels and aluminium alloys with argon shielding, using electrode wires of 1.6 mm diameter

Grade of steel or alloy	Sample thickness δ, mm	Welding speed, m/min	Constricted arc current, I_p, A	Constricted arc voltage, U_p, V	Plasma gas flow rate, Q_p, l/min	Consumable electrode arc current, I_{MIG}, A	Consumable electrode arc voltage, U_{MIG}, V	Electrode wire feed rate, v_w, m/min
SUS304	12.0	0.25	240	39	7	300	28	7.5
Steel 20	10.0	0.25	200	37	6	240	28	8.0
5083	8.0	0.4	168	23	5	213	23	7.0
1561	5.0	0.6	115	26	5	165	18	7.6

Figure 9. Butt joint of 1561 alloy (δ = 5 mm) produced by hybrid Plasma-MIG welding in the developed robotic complex: *a* — upper bead; *b* — lower bead

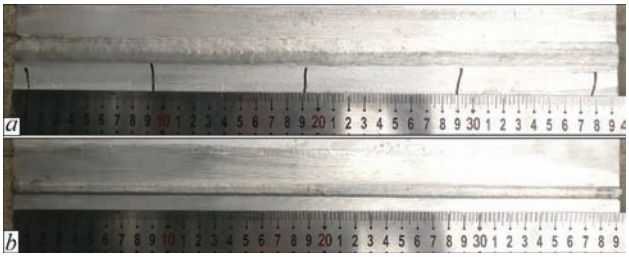

Figure 10. Butt joint of 5083 alloy (δ = 8 mm), produced by hybrid Plasma-MIG welding in the robotic complex: *a* — upper bead; *b* — lower bead

plasma-arc welding, allowing production of sound welded joints (Table).

At consumable electrode pulsed-arc welding, welding current is directly proportional to electrode wire feed rate. This causes in some cases the need to perform edge preparation to accommodate molten electrode metal. In hybrid consumable electrode plasma-arc welding with coaxial feed of electrode wire, the electrode wire feed rate can be reduced to values, required to form the geometry of penetration and convexity of the weld, in keeping with normative document requirements, by selection of the ratio of energy of nonconsumable electrode constricted arc and energy of consumable electrode arc. At application of the developed technology, there is no need to perform edge preparation for welding structures from steels and aluminium alloys with 5–12 mm wall thickness. Moreover, as shown by comparison of the derived results with those of consumable electrode arc welding, weld width and reinforcement in hybrid plasma-arc welding are reduced to 40 %.

Another result of comparison of robotic hybrid plasma-arc process with processes of plasma and MIG/MAG welding is determination of the possibility of increasing the welding speed by 25–40 %. The level of longitudinal and transverse deformations is decreased due to increasing the welding speed and reducing the quantity of deposited electrode metal. So, for 1561 alloy at the same values of welding speed, the level of longitudinal deflection of the sample at hybrid plasma-arc welding is reduced 3 times, compared to the sample, made by consumable electrode pulsed-arc welding.

Conclusions

1. Proceeding from the results, obtained at modeling of the process of hybrid consumable electrode plasma-arc welding with coaxial feed of electrode wire, equipment and basic technologies were developed for robotic welding of structures from steels and aluminium alloys with 5–12 mm wall thickness.

2. Developed control system of the complex allows synchronizing operation of two welding sources and auxiliary equipment with the actions of anthropomorphous industrial robot for realization of the process of hybrid consumable electrode plasma-arc welding.

3. Application of the developed robotic complex of hybrid plasma-arc welding and process of welding steels and aluminium alloys 5–12 mm thick allows increasing welding speed by 25–40 %, compared to consumable electrode pulsed-arc welding and reducing by 40 % the quantity of electrode wire, required for welded joint formation, in keeping with the normative documents, as well as lowering the level of residual welding deformations of welded items.

The work was performed with the support of the program of State Administration of Foreign Experts No. WQ20124400119 «1000 Talents» (PRC), Guangdong Innovative Research Team (PRC) No. 201101C0104901263, Project of Guangdong Academy of Sciences (PRC) «Capacity-building of innovation-driven development for special fund

projects» 2017GDASCX-0411; Projects of Guangdong Province (PRC) No. 2015A050502039 and 32016B050501002.

1. Skhirtladze, A.G., Bochkarev, S.V., Lykov, A.N. et al. (2013) *Automation of technological processes*. Moscow: LLC TNT.
2. Vodovozov, V.M., Myadzel, V.N., Rassudov, L.N. (1986) *Robots in ship hull productions (Control, teaching, algorithmization)*. Moscow: Sudostroenie.
3. Ovchinnikov, V.V. (2012) *Equipment, mechanization and automation of welding processes*. Practical work. Moscow: Academiya.
4. Essers, W.G., Jelmorini, G. (1975) *Method of plasma-MIG-welding*. Pat. US3891824. U.S. Philips Corp., USA.
5. Essers, W.G., Liefkens, A.C. (1972) Plasma-MIG welding developed by Philips. *Machinery and Production Eng.*, **12**, 632–633.
6. Essers, W.G., Willemes, G.A. (1984) Plasma-MIG-Schweissen von Aluminium Aufragschweissen und Zweielektrodenschweissen, von autahl. DVS-Berichte, **90**, 9–14.
7. Dedyukh, R.I. (2014) Specifics of consumable electrode plasma welding process (Review). *Svarochn. Proizvodstvo*, **5**, 34–39.
8. *Tao* Yang, Hongming Gao, Shenghu Zhang et al. (2013) The study on plasma-MIG hybrid arc behaviour and droplet transfer for mild steel welding. *Rev. Adv. Mater. Sci*., **33**, 459–464.
9. Sydorets, V.N., Zhernosekov, A.M. (2004) Numerical simulation of the system of power source-consumable-electrode arc. *The Paton Welding J*., **12**, 9–15.
10. Korzhyk, V., Grynuk, A., Khaskin, V. et al. (2016) The hybrid plasma-arc welding of thin-walled panels made of aluminum alloy. *First Independent Sci. J*., **12/13**, 28–36.
11. Ton, H. (1975) Physical properties of the plasma-MIG welding arc. *J. Phys. D: Appl. Phys*., **8**, 922–933.
12. Hertel, M., Fuessel, U., Schnick, M. (2014) Numerical simulation of the plasma-MIG process – interactions of the arcs, droplet detachment and weld pool formation. *Welding in the World*, **58**, 85–92.
13. Yang, T., Xu, K., Liu, Y. et al. (2013) Analysis on arc characteristics of plasma-MIG hybrid arc welding. *Transact. China Welding Inst*., 34(**5**), 62–66.
14. Kornienko, A.N., Makarenko, N.A., Granovskij, A.V. et al. (2001) A universal source for plasma-MIG surfacing and welding. *Svarochn. Proizvodstvo*, **9**, 25–26.
15. Oliveira, M.A. de, Dutra, J.C. (2007) Electrical model for the plasma-MIG hybrid welding process. *Welding & Cutting*, 6(**6**), 324–328.
16. Pentegov, I.V., Sidorets, V.N. (1990) Energy parameters in a mathematical model of a dynamic welding arc. *Welding International*, 4(**4**), 272–275.
17. Pentegov, I.V., Sydorets, V.N. (2015) Comparative analysis of models of dynamic welding arc. *The Paton Welding J*., **12**, 45–48.
18. Pentegov, I.V., Sydorets, V.N. (1991) Quasistatic and dynamic volt-ampere characteristics and time constant of blown and moving arcs. *Ibid*., **3**, 361–364.
19. Gao, H.-M., Bai, Y., Wu, L. (2008) Comparison between plasma-MIG and MIG procedures on 5A06 Aluminum Alloy. *Mat. Sci. Forum*, **575–578**, 1382–1388.
20. Matthes, K.-J., Kohler, T. (2002) Electrical effects and influencing quantities in the case of the hybrid plasma-MIG welding process. *Welding & Cutting*, **2**, 87–90.

Received 11.05.2017